Contents lists available at ScienceDirect

Transactions of Nonferrous Metals Society of China

36(2026) 1000−1014

www.tnmsc.cn

Electrochemical separation of Mn(II) impurity from molten salt electrolyte for magnesium electrolysis

Zhi-wen ZHAO, Zheng ZENG, Yan-ping WANG, Pei TANG, Chang JIANG, Zhong-sheng HUA*

School of Metallurgical Engineering, Anhui University of Technology, Ma'anshan 243032, China

Abstract: The electrochemical separation of Mn(II) impurity from molten NaCl−KCl−$MgCl_2$ was systematically investigated to facilitate the electrolytic production of high-purity magnesium. The reduction of Mn(II) to Mn metal on tungsten electrode was a quasi-reversible process controlled by diffusion. The apparent standard potential and exchange current density of Mn(II)/Mn(0) electrode reaction were determined at temperatures ranging from 973 to 1048 K. Solid Mn metal generated during electrolysis aggregated into irregular clumps and adsorbed some needle-like MgO, imposing a detrimental effect on both the aggregation and the purity of magnesium metal. After electrolysis at −1.5 V in molten NaCl−KCl−$MgCl_2$−0.62wt.%$MnCl_2$ for 8 h, the concentration of $MnCl_2$ impurity decreased to 0.037 wt.%, achieving a removal efficiency of 94.14%. When direct electrolysis was performed in molten NaCl−KCl−$MgCl_2$−0.62wt.%$MnCl_2$, the obtained magnesium metal was small blocks with a caviar-like appearance, and the purity was just 98.59%. In contrast, a large globule of magnesium metal was obtained when electrolysis was performed in the purified electrolyte, and its purity was improved to 99.94%. The controlled-potential electrolysis proposed in this work has been verified to be a green and practically effective method to separate the metal ion impurities from molten electrolyte for high purity magnesium extraction.

Keywords: electrochemical separation; Mn(II) impurity; high purity magnesium; removal efficiency; molten salt electrolyte

1 Introduction

Magnesium is well-known for its excellent properties and has been widely applied in the automotive, aerospace, 3C (computer, communication and consumer electronics) and other industrial fields in the world [1−4]. The global magnesium market is growing at a compound annual growth rate of about 5%, and is forecasted to reach 1.6×10^6 t by 2027 [5]. The electrolytic technology based on the molten salt electrolysis of anhydrous magnesium chloride or carnallite [6], is one of the two main techniques for the industrial production of metallic magnesium on a worldwide scale due to the significant advantages such as continuous operation, relatively low energy consumption, large-scale production, and more environmental friendliness [7]. Since $MgCl_2$ has an inexhaustible supply from brines, the electrolytic technology is considered to have greater application prospects in the future.

The impurities, especially the metal ion impurities such as Fe, Ni, Mn, Cu, and Al ions, are detrimental to both the magnesium purity and current efficiency [8]. The elimination of ionic impurities is necessary for the electrolytic magnesium production. On the other hand, electrorefining in molten salts is practicable for the recycling of magnesium metal, which is regarded as a crucial technology to expand the usage of magnesium in the future and fits well with the concept of green chemistry regarding the circular economy and near zero-emission [9]. There

Corresponding author: *Zhong-sheng HUA, Tel: +86-555-2311571, E-mail: huazs83@163.com

https://doi.org/10.1016/S1003-6326(25)67012-9

Received 12 July 2024; accepted 7 March 2025

is no doubt that some other metal impurities are contained in the magnesium scrap, and their contamination of magnesium metal should be properly controlled in the electrorefining process. Therefore, the investigation on the electrochemical behavior of impurity elements is of great importance to both the electrolytic production of magnesium metal and the electro-recycling of magnesium scrap.

The electrochemical behaviors of Fe, Ni, Mn, Cu and Al have been extensively explored in melts consisting of alkali metal chlorides [10−18]. However, the electrolysis and electrorefining of magnesium are usually conducted in the melts containing $MgCl_2$ as a main ingredient, such as the NaCl−KCl−$MgCl_2$ system or the NaCl−$CaCl_2$−$MgCl_2$ system. The reported results may not be entirely accurate or applicable to the molten salt system for magnesium electrolysis, since both the chemical and physical properties vary among different systems. Only a few studies, focusing on the electrochemical behaviors of Fe, Ni, and Cr, have been conducted in the molten salt system for magnesium electrolysis [19−22]. $MnCl_2$ is a common impurity in the chloride raw materials for electrolytic magnesium production, and thus Mn(II) is introduced into the electrolyte as a typical impurity ion [21,23]. So far, the details on electrochemical behavior and separation of Mn(II) in the electrolyte for magnesium electrolysis have not yet been fully clarified.

In this study, the electrochemical behavior of Mn(II) and its impact on the aggregation and purity of magnesium metal were thoroughly examined in the NaCl−KCl−$MgCl_2$ system. Consequently, a new method based on controlled-potential electrolysis was proposed to separate metal ion impurities from the molten salt electrolyte, and it was verified to be an effective approach for the purification of molten salt electrolyte due to its technical, economic, and environmental benefits. This work will provide further insights into the electrochemistry of impurity ions in molten salt electrolysis of magnesium metal, as well as lithium, calcium, and beryllium metals, and may also lay a theoretical foundation for their recycling from scraps via electrorefining technology.

2 Experimental

2.1 Chemicals and preparation of molten salt electrolyte

The molten salt electrolyte used in this research was a chloride mixture (177 g) composed of anhydrous NaCl, KCl and $MgCl_2$ in a molar ratio of 42∶42∶16. The chloride mixture was kept in a corundum crucible and heated at 473 K overnight to remove residual moisture, and then raised to 973 K and maintained for 60 min. Anhydrous $MnCl_2$ was introduced directly to the electrolyte as the source of Mn(II) without any additional treatment. All the metal chlorides used were of analytical grade and commercially available.

2.2 Experimental setup and electrochemical methods

All the electrochemical experiments were performed in a three-electrode system using an electrochemical workstation (PGSTAT 302 N) that was controlled by the software Nova 2.1. A tungsten wire (1 mm in diameter, 99.99% purity), a spectrally pure graphite rod (6 mm in diameter), and an Ag wire (1 mm in diameter, 99.99% purity) immersed in the solution of NaCl−KCl−$MgCl_2$−2.0mol%AgCl contained in a mullite tube served as the working electrode, counter electrode, and reference electrode, respectively. The lower end of the tungsten wire was polished thoroughly and cleaned before use, and the active surface area of the working electrode was calculated by determining the length that was immersed in the electrolyte after the experiment.

The electrode reaction of Mn(II) in the NaCl−KCl−$MgCl_2$ electrolyte was examined on tungsten electrode by cyclic voltammetry (CV), square wave voltammetry (SWV), chronopotentiometry (CP) and open circuit chronopotentiometry (OCP). Electrochemical separation of Mn(II) and electrolytic extraction of magnesium metal were conducted by potentiostatic electrolysis in the electrolyte at 973 K. All the electrochemical experiments were accomplished under the protection of flowing high-purity argon. After electrolysis, the deposits were extracted from the electrolyte, and then cleaned ultrasonically with ethanol or deionized water, and subsequently dried in vacuum.

2.3 Characterization

The contents of Mn and other elements in the samples were determined using an inductively coupled plasma optical emission spectrometry (ICP-OES, Avio 200). The elemental composition and chemical state were identified using X-ray photoelectron spectroscopy (XPS, NEXSA). The crystalline phases of the electrolytic products were

characterized by X-ray diffraction (XRD, D8 Advance) with Cu K_α radiation, and the microstructure and element distribution were examined with field emission scanning electron microscopy (FESEM, Mira3 XMU) equipped with X-ray energy-dispersive spectroscopy (EDS).

3 Results and discussion

3.1 Electrochemical behavior of Mn(II)

The electrochemical behavior of Mn(II) during magnesium electrolysis was initially investigated by CV on an inert tungsten electrode. Figure 1(a) represents the comparative CV curves measured on tungsten electrode before (dotted line) and after (solid line) the addition of 0.62 wt.% $MnCl_2$ to the molten NaCl−KCl−$MgCl_2$ at 973 K. Only one couple of redox peaks A/A′ appears at about −1.80 V/−1.64 V in the blue dotted line, corresponding to the Mg(II)/Mg(0) electrode reaction. After the addition of $MnCl_2$ to the electrolyte, a new couple of redox peaks B/B′ at approximately −1.30/−1.17 V appears in the forward and reverse scans, and can be ascribed to the deposition and subsequent dissolution of Mn metal. No other redox signals, except for A/A′ and B/B′, are observed in the electrochemical window. This implies that in the NaCl−KCl−$MgCl_2$ electrolyte, Mn(II) ions are directly reduced to Mn metal on a tungsten electrode through the following reaction:

$$Mn(II)+2e=Mn(0) \quad (1)$$

It is evident that the oxidation peak B′ exhibits a much higher current amplitude than the reduction peak B. This is the characteristic feature of the generation of an insoluble substance on the electrode during the reduction process. Additionally, it can be seen from Fig. 1(a) that the deposition potential of Mn metal is approximately 0.5 V more positive than that of Mg metal, and Mg does not combine with the preferentially reduced Mn metal to form Mg−Mn alloy through underpotential reduction, suggesting

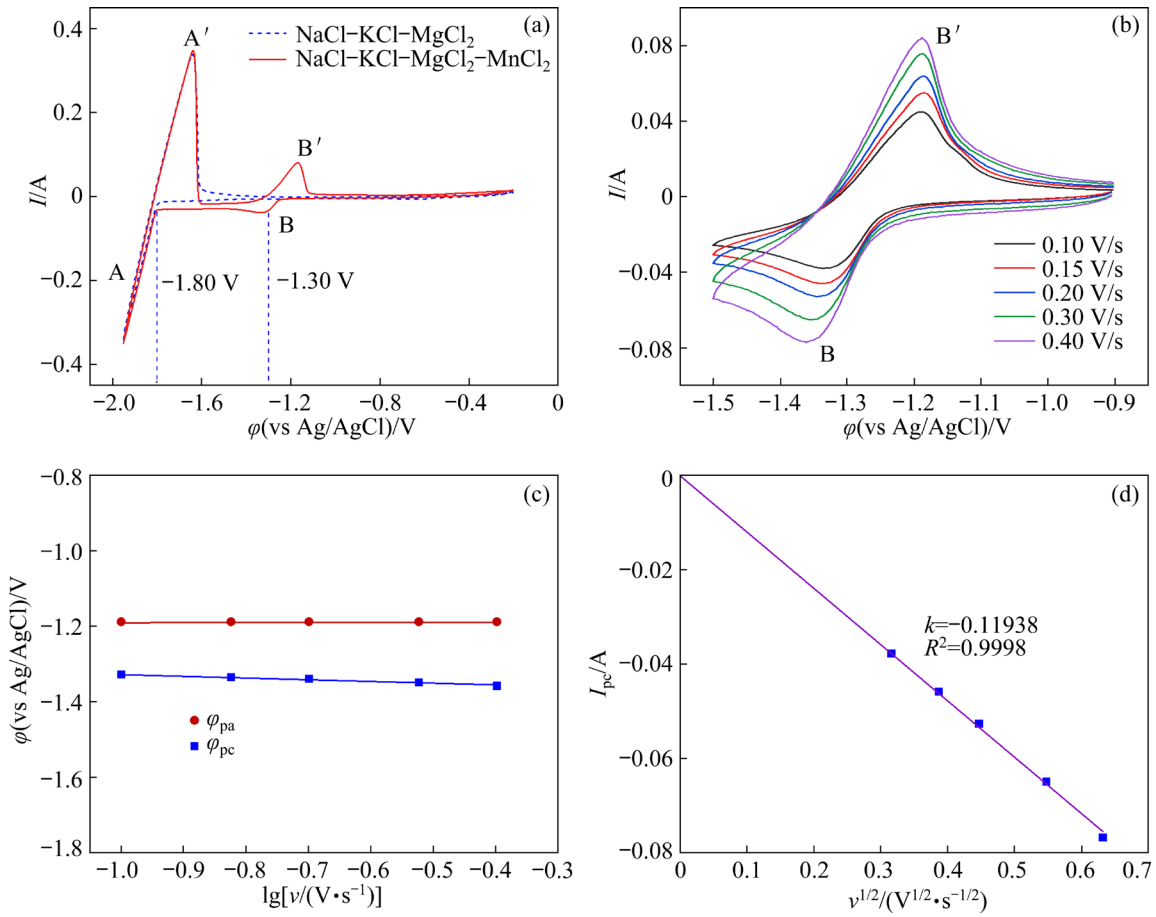

Fig. 1 CV curves measured on tungsten electrode in molten NaCl−KCl−$MgCl_2$ before and after addition of 0.62 wt.% $MnCl_2$ (a), and at different scan rates within scan range from −0.9 to −1.5 V (b); (c) Variation of peak potential versus logarithm of scan rates; (d) Relationship between cathodic peak current and square root of scan rate (Temperature: 973 K; electrode surface area: 0.322 cm^2)

that the electrochemical separation of Mn(II) impurity from the NaCl−KCl−$MgCl_2$ electrolyte should be feasible.

To explore the reversibility and control step of Mn(II)/Mn(0) electrode reaction, CV tests were performed in the molten NaCl−KCl−$MgCl_2$−0.62wt.% $MnCl_2$ with the scan rates varying from 0.10 to 0.40 V/s within the potential range from −0.9 to −1.5 V, as shown in Fig. 1(b). The curves of peak potential (φ_p) versus the logarithm of scan rate (lg v) were plotted (Fig. 1(c)). It can be seen that the anodic peak potential (φ_{pa}) exhibits a negligible excursion with the increase of scan rate, and the cathodic peak potential (φ_{pc}) displays a slight negative shift when the scan rate is higher than 0.30 V/s. Accordingly, the electrochemical reduction of Mn(II) on tungsten electrode in molten NaCl−KCl−$MgCl_2$ is considered as a quasi-reversible process [24,25]. Furthermore, the cathodic peak current (I_{pc}) increases gradually with increasing scan rate, since the diffusion layer becomes thinner at a higher scan rate. As shown in Fig. 1(d), I_{pc} is directly proportional to the square root of scan rate ($v^{1/2}$), meaning that the electrochemical reduction of Mn(II) in the molten salts is controlled by diffusion. When the reduction product is an insoluble metal, the Berzins−Delahay equation is valid for quantitatively calculating the diffusion coefficient (D) [26]:

$$I_{pc}=-0.61SC_0(nF)^{3/2}(RT)^{-1/2}v^{1/2}D^{1/2} \quad (2)$$

where S is the surface area of the working electrode immersed in electrolyte (cm^2), C_0 represents the concentration of Mn(II) ions (mol/mL), n corresponds to the number of the electrons transferred, F and R denote the Faraday's constant (96500 C/mol) and the molar gas constant (8.314 J/(mol·K), respectively, and T is the thermodynamic temperature (K). Based on the slope (k) of the fitted line in Fig. 1(d), the diffusion coefficient of Mn(II) in the NaCl−KCl−$MgCl_2$ electrolyte at 973 K is calculated to be approximately 4.4×10^{-5} cm^2/s, which is in the same order of magnitude as those reported in previous literature [15−17,27−30].

Figure 2(a) displays the SWV curves for the molten NaCl−KCl−$MgCl_2$−0.62wt.%$MnCl_2$ system at different frequencies. Only one electrochemical signal corresponding to the reduction of Mn(II) ions was detected at around −1.3 V, and the reaction is likely quasi-reversible since the reduction peak potential of SWV curves is nearly independent of

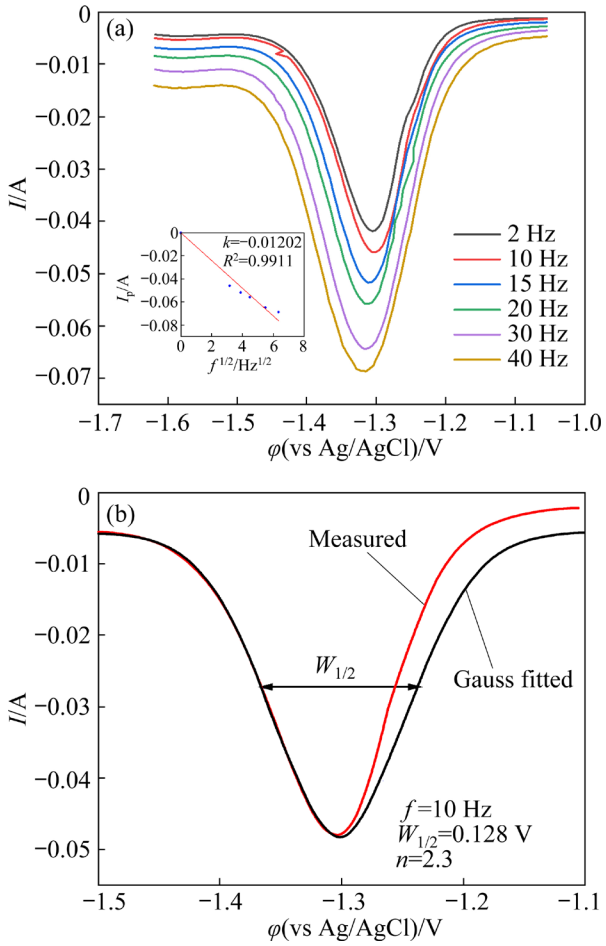

Fig. 2 SWV curves of molten NaCl−KCl−$MgCl_2$−0.62wt.%$MnCl_2$ measured on tungsten electrode at different frequencies (a) and at 10 Hz (b) (Temperature: 973 K; electrode surface area: 0.322 cm^2)

frequency. These results were consistent with those observed in CV curves. It can be seen from the inset in Fig. 2(a) that the peak current (I_p) is directly proportional to the square root of frequency ($f^{1/2}$), and the number of electrons transferred in this process can then be determined by the following formula [31]:

$$W_{1/2}=3.52\frac{RT}{nF} \quad (3)$$

where $W_{1/2}$ is the half-peak width (V). It should be noted that the shape of SWV curves is not fully symmetrical. This may be ascribed to the nucleation overpotential or nucleation effect [32,33], and consequently the increase of the current was delayed. Therefore, Gauss fitting was applied to peak B in the SWV curves by taking only left part into account when determining the half-peak width, because the left part was not affected by the nucleation effect, as

depicted in Fig. 2(b). According to this treatment method, the value of $W_{1/2}$ was measured to be 0.128 V, and the number of electrons transferred in the electrode reaction was calculated to be 2.3 (≈ 2), further confirming that the reduction of Mn(II) on tungsten electrode is a one-step process exchanging two electrons.

The electrochemical reduction of Mn(II) in molten NaCl−KCl−$MgCl_2$ was further investigated by CP, as shown in Fig. 3(a). Plateau B is attributed to the electrochemical reduction of Mn(II) to Mn metal. Afterwards, the potential rapidly shifts to a limited value of about −1.80 V, which corresponds to the reduction of Mg(II). Herein, the transition time (τ), which is the necessary time for complete consumption of the electroactive species around the electrode and attributed to the diffusion of ions in the layer of electrolyte, can be determined from CP curves according to the method described in the literature [34], as shown in Fig. 3(b). Therefore, the

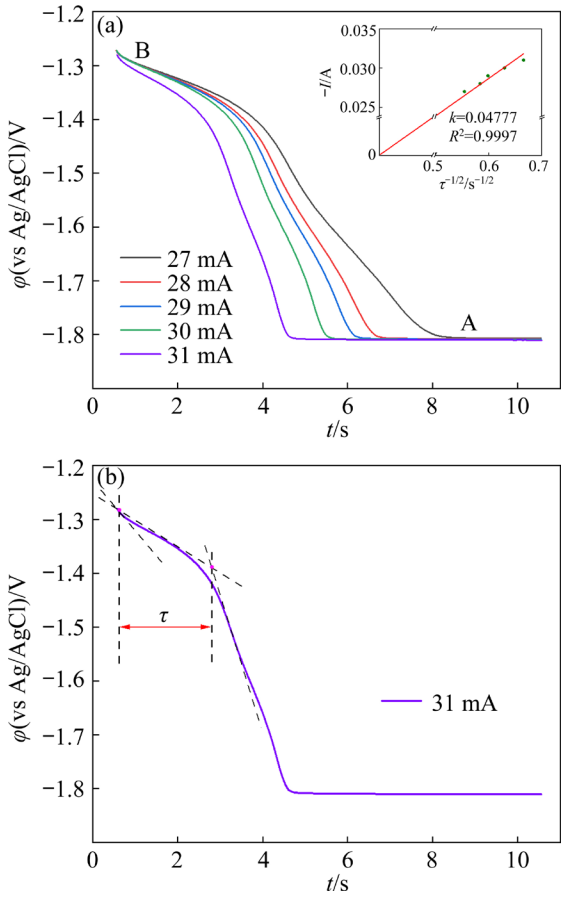

Fig. 3 CP curves for molten NaCl−KCl−$MgCl_2$−0.62wt.%$MnCl_2$ attained on tungsten electrode with various applied currents (a) and applied current of 31 mA showing determination of transition time (b) (Temperature: 973 K; electrode surface area: 0.322 cm^2)

transition time for Mn(II) reduction decreases naturally as the applied current increases. The correlation of inverse square root of transition time ($\tau^{-1/2}$) with the applied current (I) shows a good proportional relationship (shown in the inset of Fig. 3(a)). Consequently, the diffusion coefficient (D) of Mn(II) can also be estimated from the slope of the fitted line based on Eq. (4) [35]:

$$I\tau^{1/2}=0.5nFC_0S\pi^{1/2}D^{1/2} \tag{4}$$

The diffusion coefficient of Mn(II) calculated by Eq. (4) is about 8.0×10^{-5} cm^2/s. The value is larger than the one calculated by CV, but they are in the same order of magnitude. The discrepancy may be related to the combination of experimental conditions and testing methods [36].

The apparent standard potential is an important thermodynamic parameter and is often employed to probe the electrochemical reactivity of ions in the electrolyte [37]. In this case, the standard electrode potential of Mn(II)/Mn(0) ($\varphi^{0}_{Mn(II)/Mn(0)}$ vs Ag/AgCl) can be determined by the Nernst equation:

$$\varphi^{eq}_{Mn(II)/Mn(0)}=\varphi^{0}_{Mn(II)/Mn(0)}+\frac{RT}{nF}\ln\frac{a_{Mn(II)}}{a_{Mn(0)}} \tag{5}$$

where $\varphi^{eq}_{Mn(II)/Mn(0)}$ means the equilibrium potential of Mn(II)/Mn(0) couple (V), and $a_{Mn(II)}$ and $a_{Mn(0)}$ denote the activities of Mn(II) and Mn metal, respectively. The activity of pure Mn metal is equal to 1.

The apparent standard potential of Mn(II)/Mn(0) couple ($\varphi^{*0}_{Mn(II)/Mn(0)}$) has the following relationship with the standard electrode potential:

$$\varphi^{*0}_{Mn(II)/Mn(0)}=\varphi^{0}_{Mn(II)/Mn(0)}+\frac{RT}{nF}\ln\gamma_{Mn(II)} \tag{6}$$

where $\gamma_{Mn(II)}(=a_{Mn(II)}/X_{Mn(II)})$ stands for the activity coefficient of Mn(II), and $X_{Mn(II)}$ is the concentration of Mn(II) in the electrolyte. Combining Eqs. (5) and (6), $\varphi^{*0}_{Mn(II)/Mn(0)}$ can be calculated based on the following equation:

$$\varphi^{*0}_{Mn(II)/Mn(0)}=\varphi^{eq}_{Mn(II)/Mn(0)}-\frac{RT}{nF}\ln X_{Mn(II)} \tag{7}$$

Therefore, $\varphi^{eq}_{Mn(II)/Mn(0)}$ should be determined beforehand. OCP method is an appropriate method that is often utilized to determine the equilibrium potential in the molten salt system [37−40]. In this work, Mn metal was initially deposited on the tungsten electrode by potentiostatic electrolysis at −1.5 V for 100 s. Then, the current was turned off

and the variation of electrode potential with time was recorded versus the Ag/AgCl reference electrode. As shown in Fig. 4(a), a stable potential plateau corresponding to the equilibrium potential of Mn(II)/Mn(0) can be obtained at each temperature. Table 1 summarizes the equilibrium potentials measured on tungsten electrode by OCP at different temperatures. It indicates that an increase in temperature results in a slight positive shift of the equilibrium potential, suggesting that high temperature is favorable for the reduction of Mn(II). Furthermore, the apparent electrode potentials (vs Ag/AgCl) at different temperatures can be calculated by resolving Eq. (7) and are also summarized in Table 1. According to the data, the temperature dependence of the apparent standard potential of Mn(II)/Mn(0) (Fig. 4(b)) in the present work can be expressed as follows:

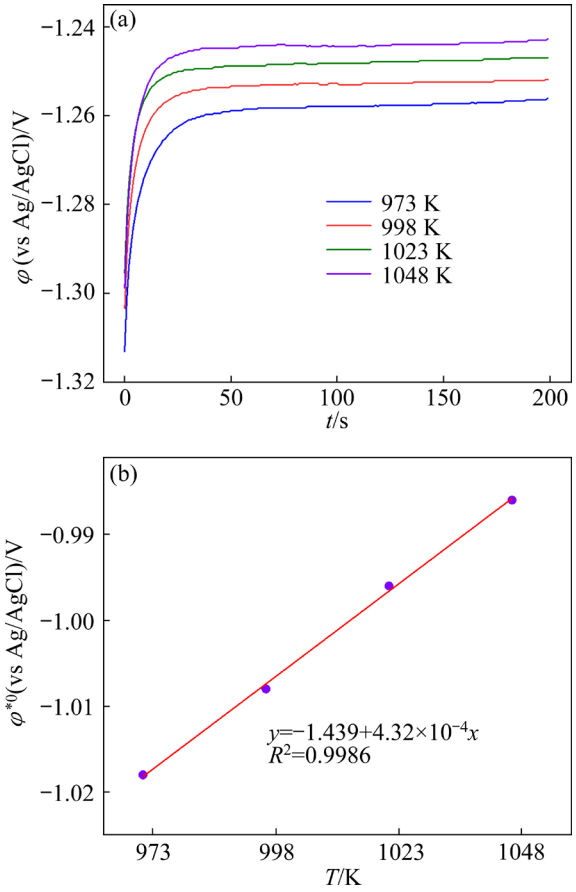

Fig. 4 (a) OCP curves measured on tungsten electrode at different temperatures in molten NaCl−KCl−$MgCl_2$−0.62wt.%$MnCl_2$ after potentiostatic electrolysis at −1.5 V for 100 s; (b) Variation of apparent electrode potential of Mn(II)/Mn(0) with temperature (Electrode surface area: 0.322 cm^2)

Table 1 Equilibrium potential, apparent standard electrode potential and exchange current density (J_0) of Mn(II)/Mn(0) redox couple in molten NaCl−KCl−$MgCl_2$ at different temperatures

T/K	φ^{eq} (vs Ag/AgCl)/V	φ^{*0} (vs Ag/AgCl)/V	J_0/(mA·cm^{-2})
973	−1.256	−1.018	7.68
998	−1.252	−1.008	9.9
1023	−1.247	−0.996	10.05
1048	−1.243	−0.986	10.88

$$\varphi^{*0}_{Mn(II)/Mn(0)}(\text{vs Ag/AgCl})=-1.439+4.32\times10^{-4}T \quad (8)$$

It is noteworthy that the apparent electrode potential of Mn(II)/Mn(0) couple (vs Cl_2/Cl^-) cannot be further calculated since the potential (vs Ag/AgCl) measured in this work cannot be converted to the potential (vs Cl_2/Cl^-).

Exchange current density is an important electrochemical parameter representing the kinetic characteristics of the reaction at the electrode/solution interface in the equilibrium state. A lower exchange current density implies that a slow redox reaction occurs while a higher value means the opposite. The magnitude of exchange current density also has a significant impact on the nucleation and the growth processes of electrodeposition, and consequently on the morphology and structure of the deposits. Electrodeposition with a high exchange current density typically results in a needle-like morphology, while a low exchange current density leads to a compact morphology [41]. Exchange current density is often determined using the Butler−Volmer equation, which can be simplified into two different equations depending on the magnitude of the overpotential applied [42]. To prevent the electrode surface from being completely covered by solid Mn metal, the linear polarization technique was adopted in this work to determine the exchange current density by applying a low overpotential. The simplified formula can be described as follows:

$$J=J_0\frac{nF}{RT}\eta \quad (9)$$

where J and J_0 stand for the net current density (A/cm^2) and the exchange current density (A/cm^2), respectively, and η is the overpotential (V), equal to the magnitude of the electrode potential deviating from the equilibrium potential.

Figure 5 displays the linear polarization curves

of Mn(II)/Mn(0) in molten NaCl−KCl−$MgCl_2$−0.62wt.%$MnCl_2$ at various temperatures. There is a well-defined linear relationship between J and η, as shown in the inset of Fig. 5. According to the slope acquired from the fitted linear polarization curves, the J_0 of Mn(II)/Mn(0) electrode reaction at different temperatures can be estimated by employing Eq. (9) and is listed in Table 1. The value of J_0 increased from 7.68 to 10.88 mA/cm^2, indicating a progressive promotion of electrode reaction with the temperature increasing from 973 to 1048 K. It confirms that rising temperature is favorable for electrochemical separation of Mn(II) impurity. It is noteworthy that J_0 is a kinetic parameter of the electrode reaction in equilibrium, which is related to the nature of the electrode reaction, reactant concentration, electrode material and temperature [11]. Due to the tiny variation of reactant concentration and surface state of the electrode, the J_0 acquired is an estimated value and may not be perfectly accurate.

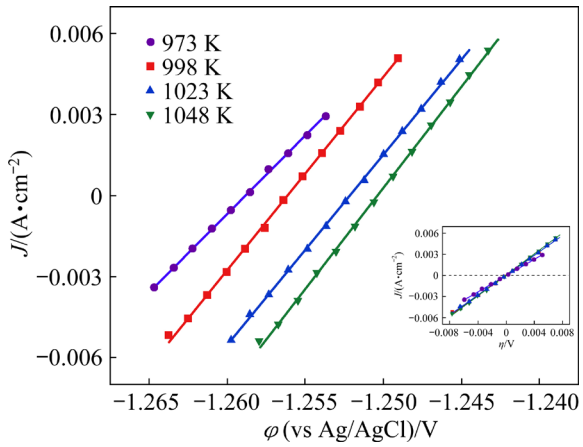

Fig. 5 Linear polarization curves acquired from molten NaCl−KCl−$MgCl_2$−0.62wt.%$MnCl_2$ after potentiostatic electrolysis at −1.5 V for 100 s with inset showing relationship between J and η (Electrode surface area: 0.322 cm^2)

3.2 Stability of Mn(II) in molten NaCl−KCl−$MgCl_2$ electrolyte

In this work, only one redox couple, Mn(II)/Mn(0), is present within the electrochemical window ranging from −0.20 to −1.95 V, as depicted in Fig. 1, signifying that Mn(II) is stable in molten NaCl−KCl−$MgCl_2$ at 973 K and will not be further oxidized to the cation with a higher valence state such as Mn(IV), Mn(VI) or Mn(VII) during the electrochemical process. To further ascertain the stability of Mn(II) ions in the electrolyte system, the presence of manganese in molten NaCl−KCl−$MgCl_2$−$MnCl_2$ was examined using XPS analysis. Figure 6(a) displays the XPS survey spectrum of NaCl−KCl−$MgCl_2$−$MnCl_2$, which was directly sampled from the molten salt electrolyte after chilling. It reveals the existence of Na, K, Mg, Mn, Cl and O elements, as determined by the binding energy values calibrated against C 1s at 284.60 eV. In addition to the first five elements, the presence of O element is likely attributed to the deliquescence of the anhydrous chlorides due to their high propensity to absorb moisture.

The surface chemical states were analyzed by multi-peak fitting, and the deconvoluted XPS spectra of Mn 2p, Mg 1s, and Cl 2p are illustrated in Figs. 6(b−d), respectively. The high-resolution XPS spectrum of Mn 2p (Fig. 6(b)) comprises two main peaks at about 641.4 and 653.0 eV, corresponding to Mn $2p_{3/2}$ and Mn $2p_{1/2}$ spin-orbit doublets, respectively. These binding energies are associated with the characteristics of Mn species in the +2 valence state [43], and the satellite peak at 646.2 eV is assigned to the chemical state of Mn^{2+} in chlorides [44]. The Mg 1s spectrum (Fig. 6(c)) can be deconvoluted into two peaks at 1302.9 and 1304.8 eV. The strong peak at 1304.8 eV represents the Mg element present in $MgCl_2$ [45], while the small peak at 1302.9 eV is ascribed to the +2 chemical state in $Mg(OH)_2$ [46], derived from the hydrolysis of $MgCl_2$. The high-resolution XPS spectrum of Cl 2p in Fig. 6(d) consists of three peaks. The prominent peak located at 198.7 eV is attributed to the Cl $2p_{1/2}$ of Cl^- [47], and the small peaks at 196.8 and 200.6 eV are assigned to the Cl $2p_{3/2}$ of Cl^- [48]. In particular, these binding energies are correlated with the existence of metal chlorides such as NaCl and $MgCl_2$ [49]. This coincides well with the fact that the molten salt electrolyte adopted in this study is composed of chlorides. Therefore, it can be reasonably concluded that Mn(II) can stably exist in the molten NaCl−KCl−$MgCl_2$ electrolyte at 973 K.

3.3 Electrochemical separation of Mn(II) impurity

To verify the practicability of separating Mn(II) impurity from the electrolyte by electrolysis at an appropriate potential, potentiostatic electrolysis at −1.5 V was performed in NaCl−KCl−$MgCl_2$. Figure 7(a) demonstrates the current evolution during potentiostatic electrolysis in molten NaCl−

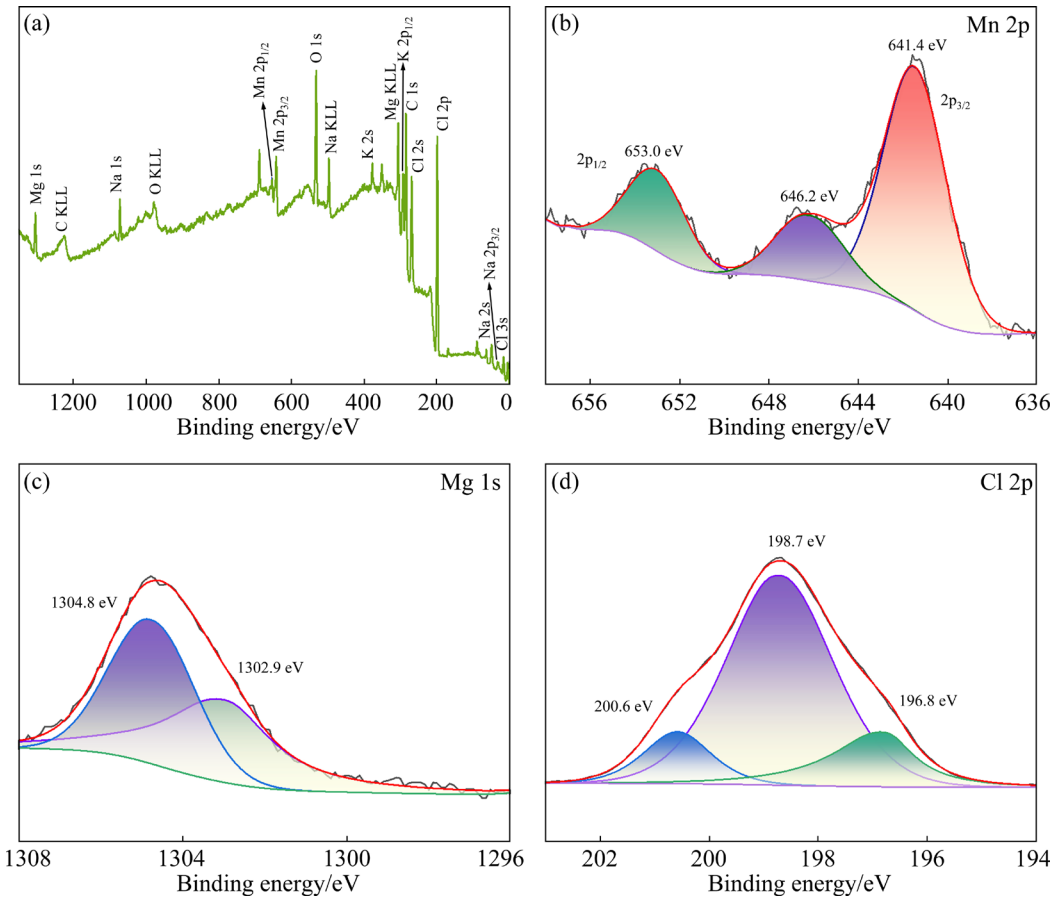

Fig. 6 XPS spectra of NaCl−KCl−$MgCl_2$−$MnCl_2$: (a) Survey spectrum; (b−d) High-resolution spectra of Mn 2p, Mg 1s, and Cl 2p, respectively

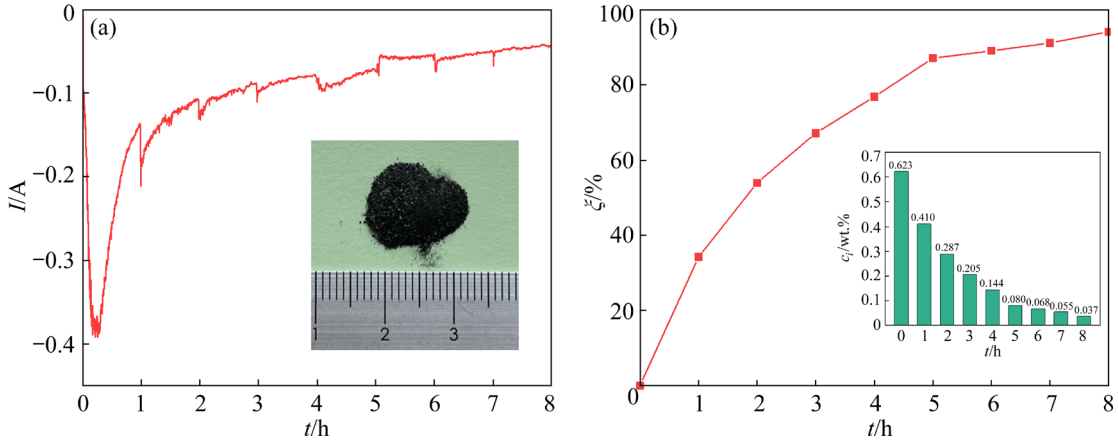

Fig. 7 (a) Current evolution recorded on tungsten electrode (surface area: 2.68 cm^2) during potentiostatic electrolysis at −1.5 V in molten NaCl−KCl−$MgCl_2$−0.62wt.%$MnCl_2$ at 973 K (Inset: The deposits obtained by potentiostatic electrolysis); (b) Variation of removal efficiency (ξ) of Mn(II) impurity with electrolysis time (Inset: The content of $MnCl_2$ (c_i) in the electrolyte at different time)

KCl−$MgCl_2$−0.62wt.%$MnCl_2$. It can be roughly divided into three consecutive stages. The current increased quickly to a maximum value in the first stage, due to the continuous deposition of Mn metal particles on the electrode, which led to a rapid increase in the electrochemical reaction area for subsequent metal deposition. After a short period, the electrolysis progressed to the second stage. The

current gradually decreased since the concentration of Mn(II) around the electrode fell to a low level due to consumption in electrolysis and the Mn(II) ions could not be sufficiently replenished by diffusion. After about 5 h, the electrolysis entered the final stage. The concentration of Mn(II) in the electrolyte dropped to a very low level due to the serious depletion after long-time electrolysis. Consequently, the current stayed at a low value and decreased only slightly in this stage. It should be noted that the current slightly fluctuated throughout the whole electrolysis process, which can likely be ascribed to the variation of the electrode surface caused by the fall-off of the solid deposits (inset of Fig. 7(a)) from the electrode. The abrupt fluctuations that occurred hourly were caused by sampling from the electrolyte during electrolysis.

To monitor the concentration variation and removal efficiency of Mn(II) impurity (ξ) during the electrolysis process, a small amount of the electrolyte was sampled directly from the electrolyte every hour for ICP-OES analysis. The removal efficiency of Mn(II) impurity (ξ) was calculated according to the following formula:

$$\xi = \frac{c_0 - c_i}{c_0} \tag{10}$$

where c_0 is the initial concentration of $MnCl_2$ in the electrolyte and c_i is the concentration after electrolysis at −1.5 V at time i. As shown in Fig. 7(b), the removal efficiency increased as the electrolysis time increased. The removal efficiency reached 53.97% rapidly within the first 2 h, and was up to 87.11% after 5 h. After 8 h of electrolysis at −1.5 V, the concentration of $MnCl_2$ impurity in the electrolyte decreased from 0.623% to 0.037%, and the removal efficiency approached 94.14%, indicating that the Mn(II) impurity can be effectively removed from the NaCl−KCl−$MgCl_2$ electrolyte by electrolysis at a suitable potential. It is noteworthy that the active surface area of the tungsten working electrode in this experiment was just 2.68 cm^2. Undoubtedly, employing a working electrode with a larger active surface area makes the electrochemical separation process significantly more efficient. From the perspective of industrial application, the cathode can be designed as a bottomless cylinder with the anode positioned vertically through its center, further improving the separation rate of Mn(II) impurity from the electrolyte.

Figure 8(a) displays the XRD pattern of the deposits extracted from the bottom of the electrolytic cell after electrolysis at −1.5 V for 8 h in molten NaCl−KCl−$MgCl_2$−0.62wt.%$MnCl_2$ system. The characteristic peaks are identified as Mn metal and MgO. This confirms that the Mn(II) impurity can be effectively separated from the NaCl−KCl−$MgCl_2$ electrolyte as Mn metal through controlled-potential electrolysis. The micromorphology and element distribution of the deposits were further examined using SEM−EDS, as shown in Figs. 8(b−e). As shown in Fig. 8(b), the granules aggregate to form irregular blocks of different sizes, with numerous needle-like structures distributed on the surface. The inhomogeneous distribution of Mn, Mg and O elements, as shown in Figs. 8(c−e), respectively, suggests that the irregular blocks are Mn metal, adsorbing some needle-like MgO on their surfaces. MgO likely originates from the insoluble MgO in the electrolyte and the hydrolysis of residual $MgCl_2$.

3.4 Impact of Mn(II) on magnesium electrolysis

Mn metal is preferentially deposited during the magnesium electrolysis process because its reduction potential is more positive, thus adversely affecting the electrolysis process. As shown in Fig. 9(a), a blackish, caviar-like product was obtained by direct electrolysis at −2.0 V in the NaCl−KCl−$MgCl_2$ electrolyte containing a high concentration of $MnCl_2$ (0.62 wt.%). ICP-OES results indicate that the impurity Mn content in the product reaches up to 1.32 wt.% (Table 2), and consequently, the purity of Mg metal is only 98.59%. There is no doubt that the Mn(II) impurity adversely affects the purity of Mg metal. It also significantly hinders the aggregation of the liquid Mg metal generated during electrolysis. Generally, the Mn(II) impurity in the electrolyte can be reduced to Mn metal through the electrochemical reaction (Reaction (1)) and the chemical process described below:

$$MnCl_2 + Mg = Mn + MgCl_2 \tag{11}$$

The generated Mn metal can precipitate with liquid Mg, causing the Mg metal to fall to the bottom of the cell due to the increased weight, thus leading to contamination and the loss of Mg metal. Furthermore, due to its high melting point (1244 °C),

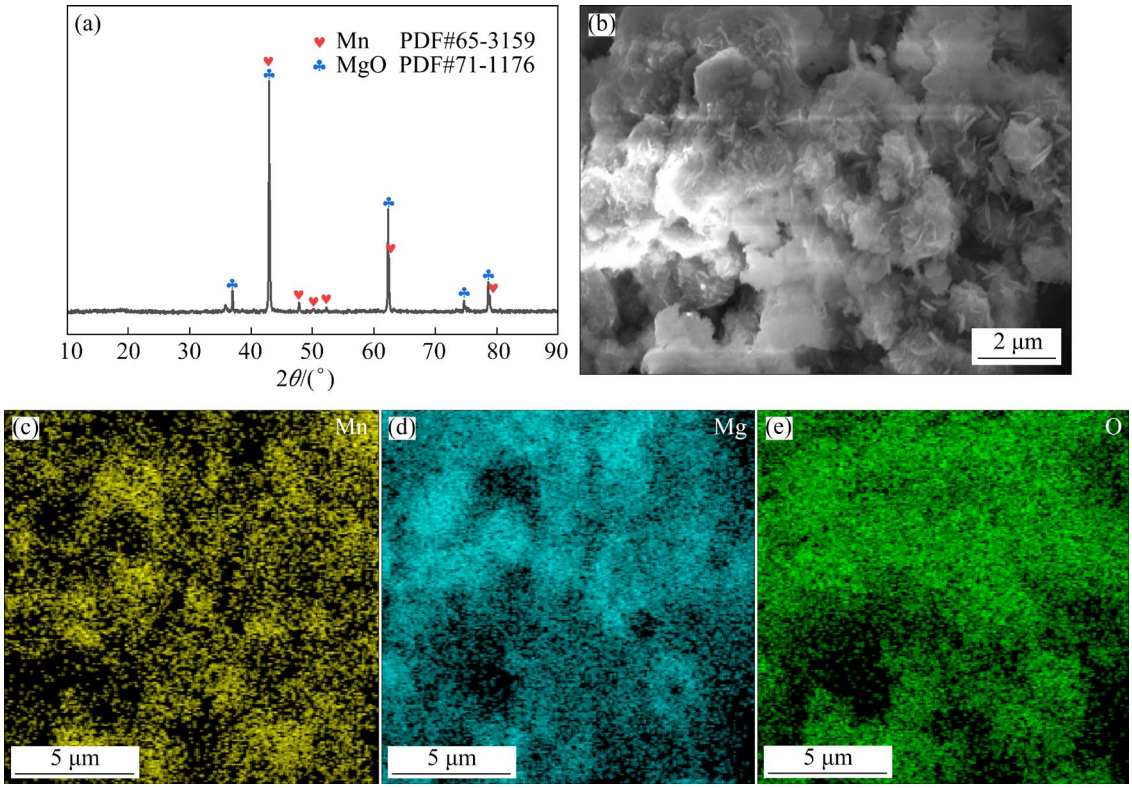

Fig. 8 XRD pattern (a) and SEM−EDS analysis results (b−e) of deposits obtained in molten NaCl−KCl−$MgCl_2$−0.62wt.%$MnCl_2$ at 973 K by potentiostatic electrolysis at −1.5 V for 8 h

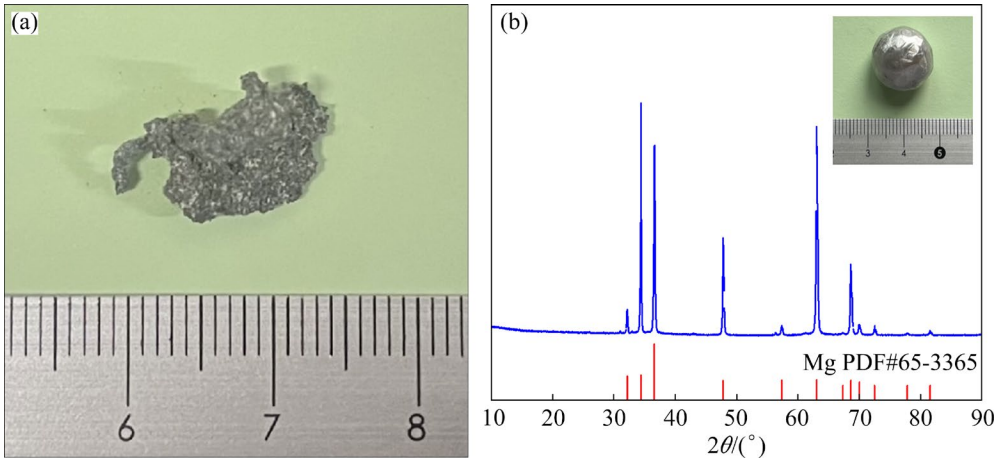

Fig. 9 (a) Metal gained at bottom of electrolytic cell by direct electrolysis at −2.0 V for 10 h in molten NaCl−KCl−$MgCl_2$−0.62wt.%$MnCl_2$ at 973 K; (b) XRD pattern of Mg metal (Inset in (b)) produced by electrolysis at −2.0 V for 10 h in electrolyte purified by pre-electrolysis at −1.5 V for 8 h

solid Mn metal was generated on the tungsten electrode. The generated Mn granules stacked together to form blocks with a three-dimensional, rough surface, as shown in Fig. 8(b), and tended to adsorb the insoluble MgO present in the NaCl−KCl−$MgCl_2$ electrolyte. The adsorption of insulative MgO is highly likely to trigger a passivation effect on the electrode. The passivation film not only degrades the electrode conductivity but also decreases the wettability of the generated liquid Mg metal on the electrode, making it difficult for the liquid Mg metal formed during electrolysis to grow and preventing it from coalescing into a larger globule. That is why a caviar-like Mg metal is obtained during direct electrolysis in the NaCl−KCl−$MgCl_2$ electrolyte containing a high concentration of Mn(II) impurity.

For comparison, potentiostatic electrolysis at −2.0 V was also carried out in the NaCl−KCl−$MgCl_2$

Table 2 Contents of typical impurities of Mg metal (wt.%)

Source	Sample	Fe	Mn	Si	Al	Cu	Ni	Mg
GB/T 3499—2011	Mg9990	0.04	0.03	0.03	0.02	0.004	0.001	99.90
	Mg9980	0.05	0.05	0.05	0.05	0.004	0.002	99.80
This work	Mg from direct electrolysis	0.0133	1.3249	0.0007	0.0399	0.0213	0.0053	98.59
	Mg from electrolysis after purification	0.0129	0.0157	0.0003	0.0212	0.0006	0.0006	99.94

electrolyte purified by pre-electrolysis at −1.5 V for 8 h. A metal ball floating on the electrolyte was obtained after electrolysis for 10 h, signifying that liquid Mg can coalesce into a large globule during electrolysis in the purified electrolyte. As shown in the inset of Fig. 9(b), the silvery luster becomes noticeable after a simple polishing treatment. The XRD pattern in Fig. 9(b) shows exclusive diffraction peaks corresponding to the Mg phase, confirming the production of Mg metal. To probe the beneficial effects of pre-electrolysis on the impurity levels in the electrolytic product, the purity of the obtained metal ball was quantitatively analyzed by ICP-OES. The main impurities found in the original magnesium ingot include Fe, Mn, Cu, Al, Ni, and Si, and their contents in the obtained Mg metal are listed in Table 2. According to the Chinese National Standard for original magnesium ingot (GB/T 3499—2011) issued by Standards Committee of China, the impurity contents conform to the specifications for product Mg9980 and approach those of Mg9990. The purity of the Mg metal obtained by electrolysis in the purified electrolyte reaches 99.94%, significantly higher than that obtained by direct electrolysis in the electrolyte containing a high concentration of Mn(II) impurity, which is only 98.59%.

3.5 Merits of controlled-potential electrolysis technology

Generally, the insoluble impurities in molten salts can be separated by filtering, while the water content can be removed by heat treatment or vacuum drying [50]. However, these technologies are ineffective for the separation of the soluble salt impurities, such as metal ion impurities. The present work verified that pre-electrolysis at −1.5 V, which is more negative than the deposition potential of impurity metal Mn, but slightly more positive than that of target extracted metal Mg, is not only effective for separating Mn(II) impurity in the NaCl−KCl−$MgCl_2$ electrolyte, but also favorable for the separation of other metal ion impurities. Thus, controlled-potential electrolysis, namely potentiostatic electrolysis at a potential between the deposition potentials of impurity metals and the target metal, proves to be an effective technology for separating metal ion impurities from molten salts.

Besides controlled-potential electrolysis, oxygen sparging and zone freezing, zeolite ion-exchange, and phosphate precipitation technologies can also be employed to remove metal ion impurities from molten salts [51−55]. Table 3 gives a brief overview of the comparison between controlled-potential electrolysis technology and the state-of-the-art technologies for molten salts purification. All of them have their own technical features. Nevertheless, they are all ex-situ technologies for molten salts purification, thus leading to the discontinuity in practical operation. On the contrary, the purification process based on controlled-potential electrolysis, which involves a shortcut reaction, can be directly performed in the electrolytic cell prior to the magnesium extraction and has distinct advantages of simpler technological steps and fewer devices. These technical features consequently bring good economic benefits. In particular, no chemical reagents are used in this process, and no waste solids or sewages are discharged. It conforms well to the criterion of green chemistry and is more environment-friendly compared with the other technologies. In conclusion, from the perspective of technical, economic, and environmental sustainability, controlled-potential electrolysis is a practically green and effective technology to purify molten salts for the electrolytic production of high purity metal and the electro-recycling of scrap metals.

Table 3 Comparison of controlled-potential electrolysis and state-of-the-art technologies for molten salts purification

Technology	Technical feature	Economic cost	Environmental impact
Controlled-potential electrolysis	One-step process and ease of scale-up for commercial operation; no external devices required; high removal efficiency for metal ion impurities; no new impurities generated	High economic benefits because of simple and continuous operation; no costs required for external devices and chemical reagents	No discharge of waste solid or sewage
Oxygen sparging and zone freezing [51]	High removal efficiency of lanthanide impurities; long time required for zone freezing; unmanageable to regulate the heating zone temperature; relatively complex technological processes and devices	High operating temperature required to obtain a high removal efficiency; energy-intensive in zone freezing process; high equipment investment and operating costs	Energy intensive in oxygen sparging and zone freezing; volatilization of hazardous salts during oxygen sparging
Zeolite ion-exchange [52,53]	High capacity for separating all fission elements; non-selective in impurity separation; low utilization efficiency of zeolite; probable to introduce new impurities	Large amounts of zeolite required to remove all the impurity species; additional costs required for disposing ceramic waste	Discharge of a large volume of ceramic waste
Phosphate precipitation [54,55]	Simple processes and easy to scale up; just effective for separation of lanthanide and actinide impurities; easy to import new impurities; slow reaction rate in solid/liquid precipitation	Consumption of phosphate reagents; extra costs required for disposing phosphates precipitation	Discharge of new solid waste

4 Conclusions

(1) The electrochemical behavior of Mn(II) impurity and its impact on magnesium electrolysis were investigated in NaCl−KCl−$MgCl_2$ electrolyte. The results indicated that the electroreduction of Mn(II) to Mn metal was a quasi-reversible, one-step process controlled by the diffusion under the experimental conditions, with the diffusion coefficient of Mn(II) calculated to be on the order of 10^{-5} cm^2/s. The apparent standard potential of Mn(II)/Mn(0) shifted positively from −1.018 to −0.986 V (vs Ag/AgCl), and the exchange current density increased from 7.68 to 10.88 mA/cm^2 as the temperature increased from 973 K to 1048 K.

(2) The feasibility of controlled-potential electrolysis for separating Mn(II) impurity from NaCl−KCl−$MgCl_2$ electrolyte was verified. After potentiostatic electrolysis at −1.5 V in molten NaCl−KCl−$MgCl_2$ containing 0.62 wt.% $MnCl_2$ for 8 h, the content of $MnCl_2$ impurity in the electrolyte decreased to 0.037 wt.%, and the removal efficiency approached 94.14%. XRD and SEM−EDS results showed that solid Mn metal was generated during electrolysis, forming irregular agglomerates of various sizes that adsorbed needle-like MgO on their surface.

(3) The Mn(II) impurity, when present in the NaCl−KCl−$MgCl_2$ molten electrolyte, exerted a detrimental impact on both the electrolysis process and the purity of the produced Mg metal. When direct electrolysis was performed in molten NaCl−KCl−$MgCl_2$ containing 0.62 wt.% $MnCl_2$, small blocks of Mg metal with a caviar-like appearance were collected, and the purity was only 98.59%. In contrast, a large globule of Mg metal was obtained from the electrolyte purified by controlled-potential electrolysis, with the purity improved to 99.94%. Controlled-potential electrolysis was proved to be a green and practically efficient technology for separating metal ion impurities from the molten electrolyte, facilitating the electrolytic production of high purity Mg metal.

CRediT authorship contribution statement

Zhi-wen ZHAO: Investigation, Validation, Writing – Original draft, Writing – Review & editing; **Zheng ZENG:** Investigation, Data curation, Writing – Review & editing; **Yan-ping WANG:** Investigation, Writing – Original draft; **Pei TANG:** Investigation; **Chang JIANG:** Investigation; **Zhong-sheng HUA:** Conceptualization, Methodology, Validation, Writing – Review & editing, Funding acquisition, Supervision.

Declaration of competing interest

The authors declare that they have no known competing financial interests or personal relationships that could have appeared to influence the work reported in this paper.

Acknowledgments

The authors are grateful for the financial supports from the National Key Research and Development Program of China (No. 2021YFC2901400), the Distinguished Young Research Project of Anhui Higher Education, China (No. 2023AH020017), and the Xinjiang Tianchi Talent Introduction Plan, China.

References

[1] GU Zuo-hong, ZHOU Yuan-xuan, DONG Quan, HE Guang-ming, CUI Jun-hao, TAN Jun, CHEN Xian-hua, JIANG Bin, PAN Fu-sheng, ECKERT J. Designing lightweight multicomponent magnesium alloys with exceptional strength and high stiffness [J]. Materials Science and Engineering: A, 2022, 855(2): 143901.

[2] KIM B, HONG C H, KIM J C, LEE S Y, BAEK S M, JEONG H Y, PARK S S. Factors affecting the grain refinement of extruded Mg−6Zn−0.5Zr alloy by Ca addition [J]. Scripta Materialia, 2020, 187: 24−29.

[3] FU Da-xue, WANG Yao-wu, DI Yue-zhong, PENG Jian-ping, FENG Nai-xiang. Factors affecting reduction efficiency in industrial retorts for Mg production by aluminothermic process [J]. Transactions of Nonferrous Metals Society of China, 2024, 34(4): 1288−1299.

[4] SONG Jiang-feng, CHEN Jing, XIONG Xiao-ming, PENG Xiao-dong, CHEN Dao-lun, PAN Fu-sheng. Research advances of magnesium and magnesium alloys worldwide in 2021 [J]. Journal of Magnesium and Alloys, 2022, 10(4): 863−898.

[5] TAN J, RAMAKRISHNA S. Applications of magnesium and its alloys: A review [J]. Applied Sciences, 2021, 11(15): 6861.

[6] GOLROUDBARY S R, MAKARAVA I, KRASLAWSKI A. Environmental assessment of global magnesium production [J]. Mineral Processing and Extractive Metallurgy Review, 2023, 44(6): 389−406.

[7] ZHAO Jia, YAN Yi-hang, ZHANG Hao, GAO Hua-yang, ZHANG Ye, LU Gui-min. Electrochemical behavior of $MgCl_2$ and co-deposition mechanisms of Mg and Sr in $SrCl_2$−KCl−$MgCl_2$ melt [J]. Transactions of Nonferrous Metals Society of China, 2024, 34(7): 2381−2392.

[8] ZHANG Yong-jian. Electrolytic metallurgy of magnesium [M]. Changsha: Central South University Press, 2006. (in Chinese)

[9] XUE Yu-dong, WANG Yun-ting. Green electrochemical redox mediation for valuable metal extraction and recycling from industrial waste [J]. Green Chemistry, 2020, 22(19): 6288−6309.

[10] KHALAGHI B, KVALHEIM E, TOKUSHIGE M, TENG Li-dong, SEETHARAMAN S, HAARBERG G M. Electrochemical behaviour of dissolved iron chloride in KCl+LiCl+NaCl melt at 550 ºC [J]. ECS Transactions, 2014, 64(4): 301−310.

[11] LIU Zhao-ting, LU Gui-min, YU Jiang-guo. Investigation on electrochemical behaviors of Ni(II) impurity in LiCl−KCl melt [J]. Separation and Purification Technology, 2021, 268: 118354.

[12] LI Shao-long, CHE Yu-si, LI Chen-yao, SHU Yong-chun, HE Ji-lin, YANG Bin, SONG Jian-xun. Study on the electrochemical behavior of Mg and Al ions in LiCl−KCl melt and preparation of Mg−Al alloy [J]. Journal of Magnesium and Alloys, 2022, 10(3): 721−729.

[13] LI Yun-gang, ZHANG Kuai, LI Jie, LIU Li-min. Electrochemical behavior of copper in the (NaCl−KCl−$CuCl_2$) molten salt [J]. Applied Mechanics and Materials, 2012, 217/218/219: 8−14.

[14] COTARTA A, BOUTEILLON J, POIGNET J C. Electrochemistry of molten LiCl−KCl−$CrCl_3$ and LiCl−KCl−$CrCl_2$ mixtures [J]. Journal of Applied Electrochemistry, 1997, 27(6): 651−658.

[15] GE Xin-lei, XIAO Sai-jun, HAARBERG G M, SEETHARAMAN S. Salt extraction process–novel route for metal extraction: Part 3 — Electrochemical behaviours of metal ions (Cr, Cu, Fe, Mg, Mn) in molten ($CaCl_2$−)NaCl−KCl salt system [J]. Mineral Processing and Extractive Metallurgy, 2010, 119(3): 163−170.

[16] CHEN Li-jun, ZHANG Min-lin, HAN Wei, YAN Yong-de, CAO Peng. Electrochemical behavior of Mn(II) in the melt LiCl−KCl−$MgCl_2$−$MnCl_2$ [J]. Chemical Journal of Chinese Universities, 2012, 33(2): 327−330. (in Chinese)

[17] XIAO Sai-jun, LIU Wei, GAO Long. Cathodic process of manganese(II) in NaCl−KCl melt [J]. Ionics, 2016, 22(12): 2387−2390.

[18] NIAZI S, OLSEN E, NYGÅRD H S. Electrochemical removal of Cu, Fe and Mn from molten $ZnCl_2$:KCl:NaCl [J]. Separation and Purification Technology, 2022, 299: 121705.

[19] TAKENAKA T, FUJITA T, KAWAKAMI M. Electrochemical behavior of impurity elements in magnesium electrolysis [J]. Materials Science Forum, 2000, 350/351: 291−298.

[20] TAKENAKA T, FUJITA T, ISAZAWA S, KAWAKAMI M. Dissolution and deposition of impurities in Mg electrolysis [J]. Materials Transactions, 2001, 42(7): 1249−1253.

[21] LIU Zhao-ting, LU Gui-min, YU Jian-guo. Effects of Fe(III) on $MgCl_2$ electrolysis and its cathodic processes on W electrodes [J]. Ionics, 2019, 25(8): 3945−3952.

[22] YANG Qiu-feng, GE Jian-bang, ZHANG Jin-suo. Electrochemical study on the kinetic properties of Fe^{2+}/Fe, Ni^{2+}/Ni, Cr^{2+}/Cr and Cr^{3+}/Cr^{2+} in molten $MgCl_2$−KCl−NaCl salts [J]. Journal of the Electrochemical Society, 2021, 168(1): 012504.

[23] YANG Zhong-yu. Metallurgy of light metals [M]. Beijing: Metallurgical Industry Press, 2013. (in Chinese)

[24] DING Li, YAN Yong-de, SMOLENSKI V, NOVOSELOVA A, XUE Yun, MA Fu-qiu, ZHANG Mi-lin. Electrochemical studies based on the extraction of Zr on Cu electrode in the LiCl−KCl molten salt [J]. Separation and Purification Technology, 2021, 279: 119683.

[25] YAO Ben-lin, LIU Kui, LIU Ya-lan, YUAN Li-yong, HE Hui, CHAI Zhi-fang, SHI Wei-qun. Raman and electrochemical

study of zirconium in LiCl−KCl−LiF−$ZrCl_4$ [J]. Journal of The Electrochemical Society, 2018, 165(2): D6−D12.

[26] BERZINS T, DELAHAY P. Theory of electrolysis at constant current in unstirred solution. II. Consecutive electrochemical reactions [J]. Journal of the American Chemical Society, 1953, 75(17): 4205−4213.

[27] LIU Shi-yuan, ZHEN Yu-lan, HE Xiao-bo, WANG Li-jun, CHOU Kuo-chih. Recovery and separation of Fe and Mn from simulated chlorinated vanadium slag by molten salt electrolysis [J]. International Journal of Minerals, Metallurgy and Materials, 2020, 27(12): 1678−1686.

[28] LIU Zhao-ting, LU Gui-min, YU Jian-guo. Investigation on electrochemical behaviors of $MnCl_2$ impurity in LiCl−KCl melts [J]. Ionics, 2021, 27(7): 2979−2988.

[29] HORVATH D, RAPPLEYE D, BAGRI P, SIMPSON M F. Electrochemical measurements of diffusion coefficients and activity coefficients for $MnCl_2$ in molten eutectic LiCl−KCl [J]. Journal of Nuclear Materials, 2017, 493: 189−199.

[30] JAFARIAN M, MALEKI A, DANAEE I, GOBAL F, MAHJANI M G. Electrodeposition of Al, Mn, and Al−Mn alloy on aluminum electrodes from molten salt ($AlCl_3$−NaCl−KCl) [J]. Journal of Applied Electrochemistry, 2009, 39(8): 1297−1303.

[31] HUA Zhong-sheng, WU Xiao-bin, ZHU Zeng-li, HE Ji-wen, HE Shi-wei, LIU Huan, XU Liang, YANG Yong-xiang, ZHAO Zhuo. One-step controllable fabrication of 3D structured self-standing Al_3Ni_2/Ni electrode through molten salt electrolysis for efficient water splitting [J]. Chemical Engineering Journal, 2022, 427: 131743.

[32] JI Nan, HUANG Wei, HAN Wei. Electrochemical behavior of Tb(III) in LiCl−KCl molten salt on liquid Zn electrode [J]. Journal of The Electrochemical Society, 2021, 168(9): 092503.

[33] ZHU Zeng-li, LIU Huan, CHEN Jie-shuang-yang, KONG Hui, XU Liang, HUA Zhong-sheng, ZHAO Zhuo. Electrochemical behavior and electrolytic preparation of lead in eutectic NaCl−KCl melts [J]. Transactions of Nonferrous Metals Society of China, 2020, 30(9): 2568−2576.

[34] HAN Wei, LI Zhu-yao, LI Mei, LI Wen-long, ZHANG Xing-mei, YANG Xiao-guang, ZHANG Mi-lin, SUN Yang. Electrochemical extraction of holmium and thermodynamic properties of Ho−Bi alloys in LiCl−KCl eutectic [J]. Journal of the Electrochemical Society, 2017, 164(4): E62−E70.

[35] BARD A J, FAULKNER L R. Electrochemical methods, fundamental and applications [M]. New York: Wiley, 2001.

[36] YAN Yong-de, ZHANG Mi-lin, XUE Yun, HAN Wei, CAO Dian-xue, HE Li-yi. Electrochemical study of the codeposition of Mg−Li−Al alloys from LiCl−KCl−$MgCl_2$−$AlCl_3$ melts [J]. Journal of Applied Electrochemistry, 2009, 39(3): 455−461.

[37] LIU Yi-chuan, LIU Ya-lan, WANG Lin, JIANG Shi-lin, WANG Dong-dong, LIU Zi-yu, LI Mei, SHI Wei-qun. Electrochemical behaviors and extraction of Ln(III) (Ln= La, Ce, Nd) ions in LiCl−KCl−CsCl eutectic salts at low temperatures [J]. ACS Sustainable Chemistry & Engineering, 2023, 11(21): 8161−8172.

[38] XI Xiao-long, WANG Ji, ZHANG Jia-yuan, LI Wen-long, NING Shun-yan, JIANG Tian-jiao, WEI Yue-zhou, HAN Wei. Electrochemical behavior and separation of Ce(III) in LiCl−KCl molten salt [J]. Separation and Purification Technology, 2024, 334: 125931.

[39] TANG Hao, PESIC B. Electrochemical behavior of $LaCl_3$ and morphology of La deposit on molybdenum substrate in molten LiCl−KCl eutectic salt [J]. Electrochimica Acta, 2014, 119: 120−130.

[40] LIU Kui, LIU Ya-lan, CHAI Zhi-fang, SHI Wei-qun. Evaluation of the electroextractions of Ce and Nd from LiCl−KCl molten salt using liquid Ga electrode [J]. Journal of the Electrochemical Society, 2017, 164(4): D169−D178.

[41] LIU Yang-yang, XU Xie-yu, SADD M, KAPITANOVA O O, KRIVCHENKO V A, BAN Jun, WANG Jia-lin, JIAO Xing-xing, SONG Zhong-xiao, SONG Jiang-xuan, XIONG Shi-zhao, MATIC A. Insight into the critical role of exchange current density on electrodeposition behavior of lithium metal [J]. Advanced Science, 2021, 8(5): 2003301.

[42] LIM K H, YUN J I. Study on the exchange current density of lanthanide chlorides in LiCl−KCl molten salt [J]. Electrochimica Acta, 2019, 295: 577−583.

[43] WANG Yun-qiu, ZHANG Xiao-ran, XI Shi-bo, XIANG Xue, DU Yong-hua, CHEN Pin-song, LYU Dan-dan, WANG Shuang-bao, TIAN Zhi-qun, SHEN Pei-kang. Rational design and synthesis of hierarchical porous Mn−N−C nanoparticles with atomically dispersed MnN_x moieties for highly efficient oxygen reduction reaction [J]. ACS Sustainable Chemistry & Engineering, 2020, 8(25): 9367−9376.

[44] MURATA S, SUZUMURA M, NAKAYAMA S, MORI-SHITA Y, NAMURA S, HATAKEYAMA M, SUNADA S. Oxidation of dibenzothiophene with molecular oxygen in the presence of aldehydes and transition metal salts [J]. Journal of the Japan Petroleum Institute, 2024, 67(1): 15−23.

[45] POKHAREL D B, WU Li-ping, DONG Jun-hua, YADAV A P, SUBEDI D B, DHAKAL M, ZHA Lin, MU Xin, UMOH A J, KE Wei. Effect of glycine addition on the in-vitro corrosion behavior of AZ31 magnesium alloy in Hank's solution [J]. Journal of Materials Science & Technology, 2021, 81: 97−107.

[46] CHENG Chun-long, CHEN Zheng, FAN Yu, WANG Lin, XU Jie, LE Qi-chi. Research on CO_2 mineralization of high temperature oxide film on magnesium alloy surface [J]. Materials Letters, 2023, 347: 134660.

[47] JIANG Lin-lin, GONG Ming-kai, JIANG Xin-yu, ZHANG Jian, LIU Guo-dong, ZENG Qing-ming. Vertical growth of 2D BiOCl nanosheets on FeOCl nanoplates as an efficient photo-Fenton catalyst for phenol degradation [J]. Desalination and Water Treatment, 2021, 225: 320−330.

[48] YANG Ruo-ting, YANG Dong-wen, WANG Meng, ZHANG Fei, JI Xin-zhen, ZHANG Meng-yao, JIA Mo-chen, CHEN Xu, WU Di, LI Xin-jian, ZHANG Yu, SHI Zhi-feng, SHAN Chong-xin. High-efficiency and stable long-persistent luminescence from undoped cesium cadmium chlorine crystals induced by intrinsic point defects [J]. Advanced Science, 2023, 10(15): 2207331.

[49] CUI Lan-yue, LI Xiao-ting, ZENG Rong-chang, LI Shuo-qi, HAN En-hou, SONG Liang. In vitro corrosion of Mg−Ca alloy: The influence of glucose content [J]. Frontiers of Materials Science, 2017, 11(3): 284−295.

[50] ONG T C, SARVGHAD M, LIPPIATT K, GRIGGS L, RYAN H, WILL G, STEINBERG T A. Review of the solubility, monitoring, and purification of impurities in molten salts for energy storage in concentrated solar power plants [J].

Renewable and Sustainable Energy Reviews, 2020, 131: 110006.
[51] CHO Y Z, LEE T K, CHOI J H, EUN H C, PARK H S, PARK G I. Eutectic (LiCl−KCl) waste salt treatment by sequencial separation process [J]. Nuclear Engineering and Technology, 2013, 45(5): 675−682.
[52] SIMPSON M F, SACHDEV P. Development of electrorefiner waste salt disposal process for the EBR-II spent fuel treatment project [J]. Nuclear Engineering and Technology, 2008, 40(3): 175−182.
[53] HARRISON M T, SIMMS H E, JACKSON A, LEWIN R G. Salt waste treatment from a LiCl−KCl based pyrochemical spent fuel treatment process [J]. Radiochimica Acta, 2008, 96(4/5): 295−301.
[54] EUN H C, KIM J H, CHO Y Z, CHOI J H, LEE T K, PARK H S, PARK G I. An optimal method for phosphorylation of rare earth chlorides in LiCl−KCl eutectic based waste salt [J]. Journal of Nuclear Materials, 2013, 442(1/2/3): 175−178.
[55] CHO Y Z, LEE T K, EUN H C, CHOI J H, KIM I T, PARK G I. Purification of used eutectic (LiCl−KCl) salt electrolyte from pyroprocessing [J]. Journal of Nuclear Materials, 2013, 437(1/2/3): 47−54.

镁熔盐电解质中杂质 Mn(II)的电化学分离

赵志稳，曾 正，王燕萍，汤 培，江 畅，华中胜

安徽工业大学 冶金工程学院，马鞍山 243032

摘 要：为了电解制备高纯度金属镁，系统研究了 NaCl−KCl−$MgCl_2$ 熔盐中杂质 Mn(II)的电化学分离。Mn(II)在钨电极上还原为金属 Mn 为受扩散控制的准可逆过程。在 973~1048 K 下测定了 Mn(II)/Mn(0)电极反应的表观标准电极电位和交换电流密度。电解过程中生成的固态金属 Mn 堆叠在一起形成了不规则的团聚物，吸附针状结构的 MgO，对金属镁的聚集性和纯度均产生了不利影响。在 NaCl−KCl−$MgCl_2$−0.62%$MnCl_2$ (质量分数)熔盐中于−1.5 V 电解 8 h 后，杂质 $MnCl_2$ 的浓度降低至 0.037% (质量分数)，杂质去除率达到 94.14%。直接在 NaCl−KCl−$MgCl_2$−0.62%$MnCl_2$ 熔盐中电解得到的金属镁块呈鱼子酱状，其纯度仅为 98.59%。相反，在净化后的熔盐中电解可得到大块的金属镁，其纯度提高到 99.94%。本文提出的控电位电解法，已被证明是分离熔盐电解质中杂质金属离子以提取高纯度金属镁的一种绿色且现实有效的方法。

关键词：电化学分离；杂质 Mn(II)；高纯度镁；去除率；熔盐电解质

(Edited by Wei-ping CHEN)